Effective Perrin theory for the anisotropic diffusion of a strongly hindered rod

T. Munk, F. Höfling, E. Frey and T. Franosch

Arnold Sommerfeld Center for Theoretical Physics (ASC) and Center for NanoScience (CeNS), Fakultät für Physik, udwig-Maximilians-Universität München, Theresienstraße 37, 80333 München, Germany

Abstract. - Slender rods in concentrated suspensions constitute strongly interacting systems with rich dynamics: transport slows down drastically and the anisotropy of the motion becomes arbitrarily large. We develop a mesoscopic description of the dynamics down to the length scale of the interparticle distance. Our theory is based on the exact solution of the Smoluchowski-Perrin equation; it is in quantitative agreement with extensive Brownian dynamics simulations in the dense regime. In particular, we show that the tube confinement is characterised by a power law decay of the intermediate scattering function with exponent 1/2.

Brownian motion of highly anisotropic particles is considerably more complex than the diffusion of spherical bjects, the basic understanding of which is founded on he seminal works by Einstein and von Smoluchowski. A shape anisotropy results in diffusion coefficients that epend on the direction of motion in the body frame, hus inducing a coupling of translation to the orientaion. This anisotropic dynamics has been investigated in ecent experiments measuring diffusion coefficients of mirometre sized ellipsoids and rods by single particle tracking [1–3]; in particular, non-Gaussian statistics has been bserved [1]. Likewise in dynamic light scattering, the otational and translational diffusion coefficients were determined simultaneously [4]. For these dilute systems, the ratio of diffusion parallel and perpendicular to the long symmetry axis was limited to values up to $D_\parallel/D_\perp \approx 4$ in quasi two-dimensional (2D) confinement.

Considerably higher values of this ratio have been observed in simulations of semi-dilute suspensions of slender rods, yielding $D_\parallel/D_\perp$ up to values of 50 [5,6]. This increase in anisotropy is caused by the steric constraints imposed by surrounding rods; thereby the transverse and rotational motion is suppressed, whereas the longitudinal transport is barely influenced [7]. An intermediate regime of anisotropic diffusion has been derived for ballistic needles within kinetic theory [8] and was observed in simulations [9].

For a finite width b, the rods undergo a phase transition to the nematic phase at densities of the order of $1/bL^2$ as predicted by Onsager [10]. The dynamics in this ordered phase becomes trivially anisotropic and splits into a fast diffusion along the nematic director axis and slower diffusion perpendicular to it. Such a pronounced anisotropic diffusion has been observed in simulations of nematic elongated ellipsoids [11] and spherocylinders [12,13]. Experiments have also clearly demonstrated orientation-dependent diffusion in colloidal nanorods in the isotropic and nematic phase [14] and in various liquid crystalline phases of *fd* viruses [15,16]. The phenomena connected with the nematic phase transition are essentially understood and will not be discussed in this work.

In the isotropic phase, experiments and computer simulations have been restricted to determine the diffusion coefficients from the mean-square displacements. The complex interplay of translational and rotational motion as exemplified for a single free ellipsoid [1] has not been studied for the strongly hindered motion in solution yet. In principle, one should characterise the dynamics in terms of an intermediate scattering function or a van Hove correlation function, as has been done recently for the smectic phase [16].

A general theory for the anisotropic motion of rods in entangled suspensions is a long-standing problem, due to the intricacy of the many-body interaction. In particular, such a theory should include memory effects from the translation-rotation coupling and explain the emergence of new macroscopic time and length scales. To account for phenomena which depend on the simultaneous interaction

with many particles, a non-perturbative approach is required. Substantial progress would be achieved in terms of an effective one-particle theory that allows for quantitative predictions.

Unhindered motion. – Already at the level of a *single, free* rod the problem is involved: the dynamics of the probability distribution $\Psi(\boldsymbol{R}, \boldsymbol{u}, t)$ is governed by the Smoluchowski-Perrin (SP) equation [17–19],

$$\partial_t \Psi = -D_{\text{rot}} \hat{L}^2 \Psi + \partial_{\boldsymbol{R}} \cdot \left[(D_\parallel - D_\perp) \boldsymbol{u} \, \boldsymbol{u} + D_\perp \mathbb{I} \right] \cdot \partial_{\boldsymbol{R}} \Psi, \tag{1}$$

with the centre of mass position of the rod $\boldsymbol{R}$, its orientational unit vector $\boldsymbol{u}$, the rotational diffusion coefficient D_{rot}, and the angular part of the Laplacian, $-\hat{L}^2$. The full formal solution of this equation in 3D was given in ref. [20]; its quantitative evaluation is still missing, although certain aspects are well understood [18, 19]. To the best of our knowledge, the solution $\Psi(\boldsymbol{R}, \boldsymbol{u}, t)$ of the Smoluchowski-Perrin equation has not been discussed for 2D systems. Equation (1) is trivially solved for isotropic diffusion, $D_\perp = D_\parallel$, and at macroscopic time scales, $t \gg 1/D_{\text{rot}}$, where the translation-rotation coupling is relaxed. Then, the second term may be averaged over $\boldsymbol{u}$, yielding the average diffusion coefficient.

Model for interacting rods. – We study a model for the sterically constrained dynamics of rods that naturally induces anisotropic diffusion of arbitrarily large ratios $D_\parallel/D_\perp$. The model is set up in a 2D environment; the dynamic properties we focus on are however equally present in a 3D embedding space. We demonstrate that the Smoluchowski-Perrin equation provides an excellent effective theory for the dynamics, when the measured diffusion coefficients serve as input parameters. In particular, we compare mean-square displacements (MSDs) and the intermediate scattering function from computer simulations with their exact results from eq. (1). Furthermore, we have discovered an intermediate algebraic decay in the intermediate scattering function, characteristic for the anisotropic sliding motion.

The model considers the overdamped motion of a single rod with zero width exploring a plane with randomly distributed, hard point obstacles [21]. Then the orientational unit vector of the rod is parametrised by one angle, $\boldsymbol{u}(t) = (\cos\vartheta(t), \sin\vartheta(t))$, and $\hat{L}^2$ reduces to $-\partial_\vartheta^2$. The model ignores any excluded volume to exclusively concentrate on entanglement effects. The physical properties of this system are thus controlled by a single parameter, the reduced density $n^* := nL^2$, where L denotes the length of the rod, and n the number density of the obstacles. The model is closely related to 3D suspensions of rods when considering a planar section. A tagged rod found initially in this plane is approximately confined to it by the neighbouring rods for times shorter than the orientational relaxation time, $t \ll \tau_{\text{rot}} := D_{\text{rot}}^{-1}$, the largest time scale present in the system [21]. The constrained motion
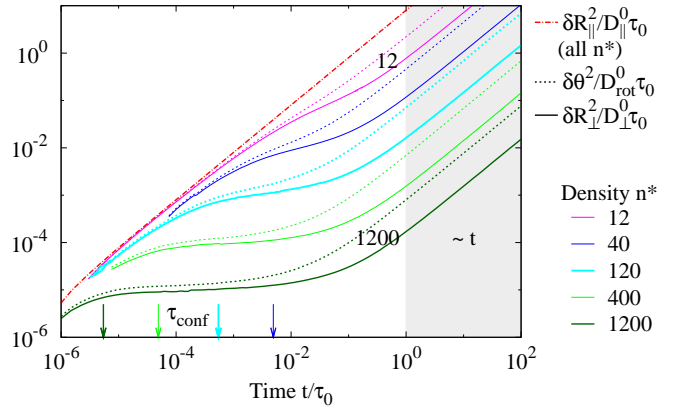

Fig. 1: (colour online) Simulated body-frame MSD in the entangled regime. For each density, three observables are shown: The MSD parallel to the rod's axis (topmost, dash-dotted), perpendicular (solid), and the MSAD (broken). Arrows at the bottom indicate τ_{conf} for the corresponding density; the diffusive regime is shaded.

of the rod then corresponds to diffusion in a planar course of localised intersection points.

Anisotropic diffusion. – The microscopic motion of the rod is diffusive, with diffusion coefficients chosen according to first order hydrodynamics of a slender rod, $D_\perp^0 = D_\parallel^0/2$, and $D_{\text{rot}}^0 = 6D_\parallel^0/L^2$. For the computer simulations we have combined the Langevin equations corresponding to eq. (1) with an event-driven algorithm to detect the collisions between rod and obstacles [21–23]. The MSDs in fig. 1 visualise essential properties of the model in the semi-dilute regime, $n^* \gg 1$. We define the displacement in the *body-fixed* frame along the axis as $\Delta R_\parallel(t) := \int_0^t \dot{\boldsymbol{R}}(t') \cdot \boldsymbol{u}(t') \mathrm{d}t'$, and similarly the transverse part $\Delta R_\perp(t)$. The parallel MSD, $\delta r_\parallel^2(t) := \langle \Delta R_\parallel(t)^2 \rangle$, is not affected by the obstacles at all, due to zero excluded volume. Consequently, the parallel diffusion coefficient is independent of the density, $D_\parallel \equiv D_\parallel^0$. In contrast, the perpendicular MSD $\delta r_\perp^2(t)$ and the mean-square angular displacement (MSAD) $\delta\vartheta^2(t)$ enter a plateau beyond a density-dependent time scale τ_{conf}. The plateau reflects the local confinement to an effective cage built up by the surrounding obstacles, referred to as "tube" [19]. Its diameter d is determined by $nLd \approx 1$, leading to a relation for the time when the confinement becomes effective, $\tau_{\text{conf}} := d^2/D_\perp^0 \approx 1/n^2L^2D_\perp^0$. At the time scale $\tau_0 = L^2/D_\parallel$, the rod moves a distance comparable to its length L, hence it leaves the tube and the MSDs become diffusive again. From the long-time asymptotes, the diffusion coefficients are read off, e.g., $D_\perp(n^*) = \lim_{t\to\infty} \partial_t \delta r_\perp^2(t)/2$. Fig. 2 demonstrates the huge suppression of perpendicular and rotational diffusion coefficients: both scale with obstacle density as n^{-2}, as has been argued by Szamel [7]. A consequence of the vanishing perpendicular component is the saturation of the centre of mass diffusion,
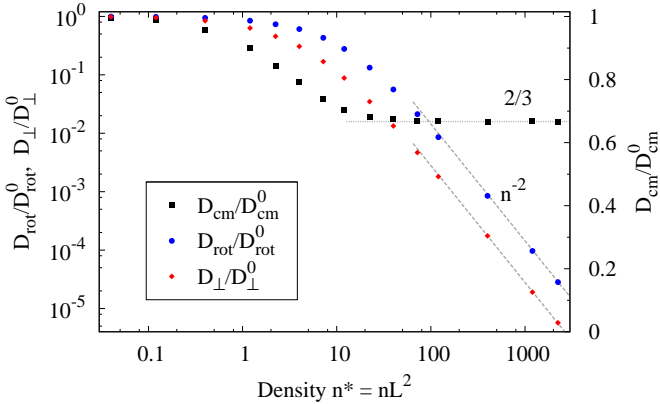
Fig. 2: (colour online) Density dependence of the diffusion coefficients. Left axis: rotational diffusion and transverse diffusion; right axis: centre of mass diffusion.
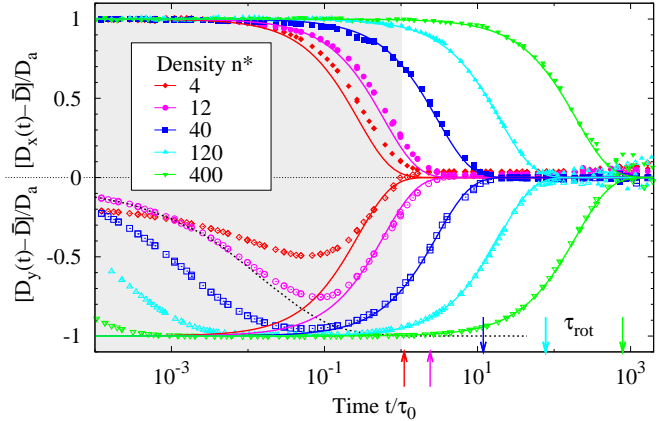

Fig. 3: (colour online) Deviations of the diffusion coefficients $D_x(t)$ and $D_y(t)$ in the space-fixed frame from the isotropic value $\bar{D}$. The initial orientation is fixed to the x-axis; normalisation is chosen such that values of ± 1 indicate diffusion with $D_\parallel$ and $D_\perp$, respectively. Symbols show results of simulations, solid lines the effective Perrin theory; arrows indicate τ_{rot} for the different densities. The broken line displays the measured $[D_\perp(t) - \bar{D}]/D_a$ at $n^* = 12$ for comparison. For $t \to 0$, the perpendicular diffusion in the simulations asymptotically approaches $[D_y(t \to 0) - \bar{D}]/D_a = [1 - D_\parallel/D_\perp(n^*)]^{-1}$.

$D_{\text{cm}}(n^* \gg 1) = 2D_{\text{cm}}^0/3$. For the largest simulated density, $n^* = 2240$, the anisotropy ratio approaches a value of $D_\parallel/D_\perp \approx 10^5$. Note that these large ratios in dense systems do not require an anisotropy on the microscale; rather the anisotropic motion is generated dynamically from the strong interaction with many obstacles.

A characteristic crossover between anisotropic and isotropic dynamics is seen clearly when plotting the time-dependent diffusion coefficients in a *space-fixed* frame, $D_x(t) := \partial_t \langle \Delta x(t)^2 \rangle_f/2$ and $D_y(t) := \partial_t \langle \Delta y(t)^2 \rangle_f/2$, where the subscript 'f' indicates that the initial orientation is fixed to the x-axis; seen fig. 3. The memory of the orientation is lost only at times larger than $\tau_{\text{rot}} \sim n^2$, resulting in a time window of anisotropic diffusion that is significantly prolonged with increasing density. Note that fig. 2 directly visualises the density dependence of the timescale indicating the crossover to isotropic dynamics, $\tau_{\text{rot}} \equiv D_{\text{rot}}^{-1}$.

For comparison with the unhindered anisotropic motion, eq. (1) is solved for the conditional probability distribution $\Psi(\mathbf{R}, \vartheta, t|\vartheta_0)$, with the initial condition $\Psi(\mathbf{R}, \vartheta, t = 0|\vartheta_0) = \delta(\mathbf{R})\delta(\vartheta - \vartheta_0)$. A Fourier transform defines the characteristic function $G_{\mathbf{k}}(\vartheta, t|\vartheta_0) = \int e^{-i\mathbf{k}\cdot\mathbf{R}} \Psi(\mathbf{R}, \vartheta, t|\vartheta_0)d\mathbf{R}$. Its equation of motion attains the form of a Schrödinger equation,

$$\partial_t G_{\mathbf{k}} = -\hat{\mathcal{H}}_0 G_{\mathbf{k}} - \hat{V} G_{\mathbf{k}}, \qquad (2)$$

with the operators $\hat{\mathcal{H}}_0 = -D_{\text{rot}}\partial_\vartheta^2$ and $\hat{V} = (D_\parallel - D_\perp)(\mathbf{k}\cdot\mathbf{u})^2 + D_\perp k^2$. Perturbation theory in $kL \ll 1$ now solves iteratively for $G_{\mathbf{k}}$. The central quantity of interest is the intermediate scattering function, $F(\mathbf{k}, t|\vartheta_0) := \int G_{\mathbf{k}}(\vartheta, t|\vartheta_0)d\vartheta$. Up to fourth order in k,

$$F(\mathbf{k}, t|\vartheta_0) = 1 - \bar{D}k^2 t - \frac{D_a}{2}\tau_4(t)\left(k_+^2 + k_-^2\right)$$

$$+ \frac{\bar{D}^2}{2}k^4 t^2 + \frac{\bar{D}D_a}{2}k^2 t\tau_4(t)\left(k_+^2 + k_-^2\right) \qquad (3)$$

$$+ \frac{D_a^2}{8D_{\text{rot}}}\left\{\frac{\tau_4(t) - \tau_{16}(t)}{6}\left(k_+^4 + k_-^4\right) + k^4[t - \tau_4(t)]\right\}.$$

The notation is abbreviated with the isotropic and anisotropic diffusion coefficients, $\bar{D} = (D_\parallel + D_\perp)/2$, $D_a = (D_\parallel - D_\perp)/2$, the wavevector components $k_\pm = (k_x \pm ik_y)e^{\mp i\vartheta_0}$, and $\tau_j(t) := \int_0^t e^{-jD_{\text{rot}}s}ds$. Note that the dependence of eq. (3) on ϑ_0 is hidden in the definition of $k_\pm$—this property originates from rotational symmetry and holds to all orders in k. From $F(\mathbf{k}, t|\vartheta_0)$ all moments are obtained by derivatives, e. g., $\langle \Delta x(t)^2 \rangle_f = -\partial_{k_x}^2 F(\mathbf{k}, t|\vartheta_0)|_{\mathbf{k}=0}$. Some of these moments have been calculated by Han et al. [1] from the Langevin equations equivalent to eq. (1).

Effective Perrin theory. – The idea is to use the solutions of the Smoluchowski-Perrin equation with the diffusion coefficients $D_\parallel, D_\perp(n^*), D_{\text{rot}}(n^*)$—measured in the simulations—to obtain a prediction for time-dependent MSDs and the intermediate scattering function in the presence of obstacles. In other words, the results from the simulations for two transport coefficients in semi-dilute systems are employed in the theory derived for *free* diffusion to describe the full time-dependence of a *semi-dilute* suspension. Since the orientation changes only gradually, the long-time rotational motion is described by diffusion [21]. Thus the description in terms of an effective Perrin theory has to be trivially correct in the relaxed regime where translational diffusion is isotropic, i.e., on macroscopic time and length scales, $t \gtrsim \tau_{\text{rot}}$ and

$k^{-1} \gtrsim L_{\rm rot} := \sqrt{D_a \tau_{\rm rot}}$.

We will show that in fact the effective Perrin theory constitutes a quantitative *mesoscopic* theory in the dense regime, $n^* \gg 1$, and successfully describes also the translation-rotation coupling induced by the interaction with the many obstacles. That such an approach should work in principle has been anticipated earlier for dense needle liquids [8]. A comparison with simulated MSDs, fig. 3, reveals excellent agreement down to the time scale τ_0. For short times, $t \ll \tau_0$, the space- and body-fixed frames coincide, implying $D_x(t) \simeq D_\parallel(t)$ and $D_y(t) \simeq D_\perp(t)$.

To access the full range of wavenumbers, we construct the exact solution of $G_{\boldsymbol{k}}(\vartheta, t|\vartheta_0)$ in terms of Mathieu functions. The equation of motion, eq. (2), is rewritten as

$$\partial_t G_{\boldsymbol{k}} = D_{\rm rot}\partial_\vartheta^2 G_{\boldsymbol{k}} - k^2\left(\bar{D} + D_a \cos 2\vartheta\right)G_{\boldsymbol{k}}, \quad (4)$$

in a coordinate frame with $\boldsymbol{k} = k\hat{e}_x$. A separation ansatz, $G_{\boldsymbol{k}}(\vartheta, t) = g_{\boldsymbol{k}}(\vartheta)\mathrm{e}^{-\lambda t}$, yields the Mathieu equation, $0 = \partial_\vartheta^2 g_{\boldsymbol{k}} + (a - 2q\cos 2\vartheta) g_{\boldsymbol{k}}$, with the parameter $q = D_a k^2 / 2D_{\rm rot}$ and the eigenvalue $a = (\lambda - \bar{D}k^2)/D_{\rm rot}$. The general solution is thus a linear combination of even and odd eigenfunctions, $\mathrm{ce}_j(\vartheta, q)$ and $\mathrm{se}_j(\vartheta, q)$ [24];[1] the decay rate $\lambda = \lambda(a, k) = aD_{\rm rot} + \bar{D}k^2$ depends on the corresponding even and odd eigenvalues, $a \to a_j(q)$ and $a \to b_j(q)$, respectively:

$$G_{\boldsymbol{k}}(\vartheta, t|\vartheta_0) = \sum_{j=0}^{\infty}\left[\mathrm{e}^{-\lambda(a_j, k)t}\mathrm{ce}_j(\vartheta_0, q)\mathrm{ce}_j(\vartheta, q)\right.$$
$$\left. + \mathrm{e}^{-\lambda(b_j, k)t}\mathrm{se}_j(\vartheta_0, q)\mathrm{se}_j(\vartheta, q)\right]. \quad (5)$$

The intermediate scattering function with unconstrained initial orientation is obtained by integrating over ϑ and ϑ_0,

$$F(\boldsymbol{k}, t) = \mathrm{e}^{-k^2 \bar{D}t}\sum_{j=0}^{\infty}\mathrm{e}^{-a_{2j}(q)D_{\rm rot}t}\left[A_0^{(2j)}(q)\right]^2, \quad (6)$$

with coefficients $A_0^{(2j)}(q) := \int_0^{2\pi}\mathrm{ce}_{2j}(\vartheta, q)\mathrm{d}\vartheta/\sqrt{2\pi}$.

The convergence of the sum is determined by the magnitude of q. The eigenvalues $a_j(q)$ are ordered ascendingly in j; furthermore, the coefficients fulfil $A_0^{(2j)}(q) = \mathcal{O}(q^j)$. Hence for $q \ll 1$, the low-j terms yield the major contributions to the sum, $F(\boldsymbol{k}, t) = \mathrm{e}^{-k^2 \bar{D}t}\left[\mathrm{e}^{q^2 D_{\rm rot}t/2}(1 - q^2/8) + \mathrm{e}^{-4D_{\rm rot}t}q^2/8 + \mathcal{O}(q^4)\right]$, representing the first correction to isotropic diffusion. Thus $q^2 \lesssim 1$ defines the macroscopic regime, corresponding to $(kL_{\rm rot})^4 \lesssim 4$, and $L_{\rm rot}$ is derived as the relevant macroscopic scale.

The opposite limit, $q \gg 1$, is relevant for large densities due to the suppression of $D_{\rm rot}$. The asymptotic expansion $a_j(q) \simeq -2q + (4j + 2)\sqrt{q} + \mathcal{O}(1)$ reveals a reduction of the exponential prefactor in eq. (6) to $\mathrm{e}^{-k^2 D_\perp t}$,

[1] We use the normalisation $\int_0^{2\pi}\mathrm{ce}_j^2(\vartheta, q)\mathrm{d}\vartheta = 1$ and $\int_0^{2\pi}\mathrm{se}_j^2(\vartheta, q)\mathrm{d}\vartheta = 1$.

and a large number of terms contribute. Then, the terminal relaxation is ruled by an exponential with decay rate $\tau_{\rm term}^{-1} := k\sqrt{2D_a D_{\rm rot}} + k^2 D_\perp$.

Based on the simulation results for the intermediate scattering function, we test the range of validity of the effective Perrin theory in fig. 4. The quality of our data, approaching a signal-to-noise ratio of 10^{-4} in the scat-
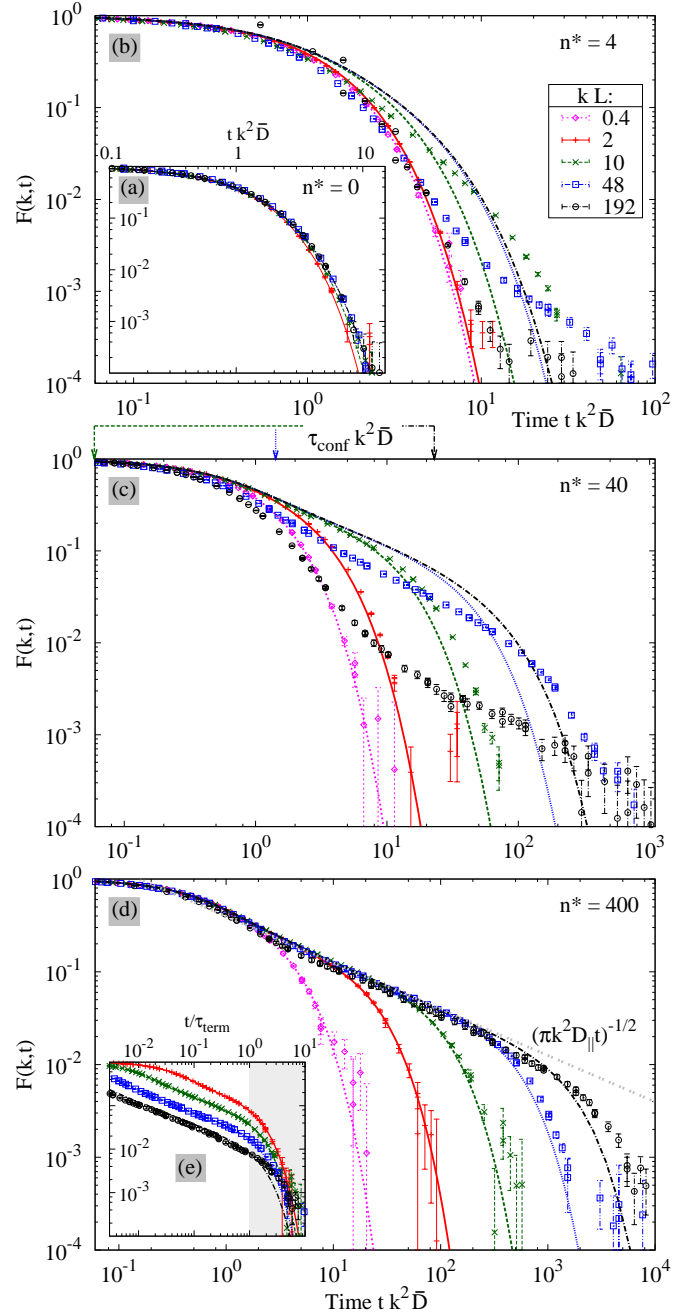

Fig. 4: (colour online) Time and wavenumber dependence of the intermediate scattering function for densities (a) $n^* = 0$, (b) $n^* = 4$, (c) $n^* = 40$, and (d), (e) $n^* = 400$. Symbols represent simulation results, lines the effective Perrin theory, eq. (6), and time is in units of $k^2\bar{D}$. By rescaling time with $\tau_{\rm term}$, inset (e) visualises the terminal relaxation.
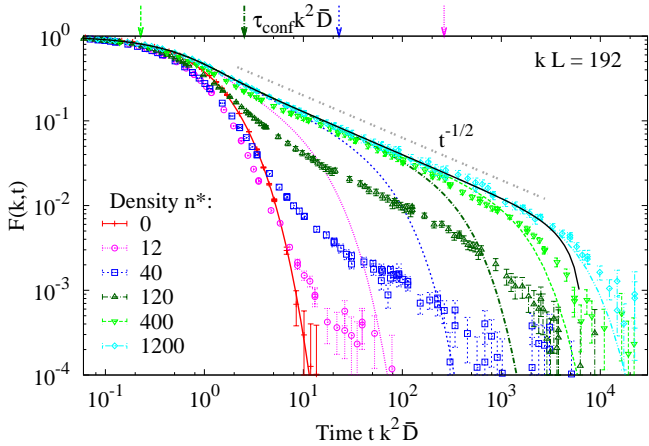
Fig. 5: (colour online) intermediate scattering function for fixed wavenumber and varying density. Increasing confinement is manifested in the simulations (symbols) by the development of a power law decay. Lines show the effective Perrin theory; the perturbative correction to eq. (7) is indicated by the thick black line for $n^* = 1200$.

tering function, allows for a clear distinction of features on a large range of time and length scales.[2] By construction, the theory describes the data at zero density [panel (a)]. For intermediate densities, $n^* \simeq 1$, the Perrin prediction strongly deviates from the simulation. The two lowest wave numbers are in the macroscopic regime; correspondingly the curves coincide after proper rescaling [panel (b)], and the Perrin prediction applies in the trivial sense. At larger densities, the agreement becomes increasingly accurate as the wave number decreases [panels (c), and (d)] also for wavenumbers beyond the macroscopic regime. Second, deviations are shifted to larger wavenumbers for higher densities. We conclude that there is a density-dependent length scale ξ determining the validity of our coarse-grained approach. From all simulated densities, we have identified ξ as the typical distance between obstacles, $\xi := n^{-1/2}$: for the shown densities, $n^* = \{4, 40, 400\}$, the corresponding wavenumbers $2\pi/\xi$ are $13L^{-1}$, $40L^{-1}$ and $126L^{-1}$, respectively. The slowing down of the dynamics with increasing confinement is displayed in fig. 5. For high wavenumbers $k \sim 2\pi/d$ the intermediate scattering function probes the formation of the tube at time scales τ_{conf}, see figs. 4c and 5. Once the tube confinement becomes effective, an intermediate algebraic decay emerges, $F(\boldsymbol{k}, t) \sim t^{-1/2}$, which we attribute to the sliding motion inside the tube. This power law is cut off by an exponential relaxation at τ_{term}, see fig. 4e.

Origin of the power law. – The power law is hidden in eq. (6) in the sum of many exponentials for $q \gg 1$. For strongly suppressed perpendicular and rotational motion,

eq. (4) is approximated by $\partial_t G_{\boldsymbol{k}} = -k^2 D_\parallel \cos^2(\vartheta) \, G_{\boldsymbol{k}}$, which yields

$$F(\boldsymbol{k}, t) = \mathrm{e}^{-k^2 D_\parallel t/2} I_0\big(k^2 D_\parallel t/2\big) \simeq \big(\pi k^2 D_\parallel t\big)^{-1/2}. \quad (7)$$

The second relation results from an expansion of the modified Bessel function of the first kind $I_0(z)$ for large argument; it quantitatively reproduces the scattering function in the power law regime, shown in fig. 4d. Perturbation theory in D_{rot} also captures the terminal relaxation with the previously calculated τ_{term}, see fig. 5.

Conclusions. – From our analysis we conclude that the motion of thin rods in concentrated suspensions exhibits a rich interplay of time and length scales, as exemplified in the MSDs and intermediate scattering function. The hindered motion leads to a strong anisotropic dynamics manifested in a significant translation-rotation coupling which persists up to macroscopic length and time scales, L_{rot} and τ_{rot}. This dynamically induced coupling is an emergent phenomenon with long memory effects. The confinement in the tube gives rise to a well separated spectrum of length scales $d \ll \xi \ll L \ll L_{\mathrm{rot}}$. The tube becomes effective once the rod encounters new steric constraints—thus the interparticle distance ξ constitutes the lower length scale of a mesoscopic window, where an effective theory with renormalized parameters becomes valid; this regime extends up to L_{rot}. Note that such a window opens only in the strongly anisotropic regime and is absent for, e.g., ellipsoids with moderate aspect ratio. There the orientational motion is dominated by excluded volume effects, and becomes neither diffusive nor exponential [25, 26]. For strongly entangled suspensions, the orientation changes only gradually by tube renewals, and it has to be included in the set of slow degrees of freedom in addition to the translation. The effective Perrin theory constitutes a Markov process in these variables, and the long memory observed in the intermediate scattering function is generated by integrating out the slowly varying orientation. This mesoscopic description is independent of the details of the tube generation; in particular, the obstacles may also fluctuate in time and space, or even disappear.

The Perrin approach fails to capture the fact that strongly confined needles have to diffuse along their axis a distance L to relax the tube constraint. However, since the rotational diffusion D_{rot} is much slower than $D_\parallel/L^2$, this appears to be negligible, at least on the scales investigated here.

We expect that our findings are also relevant for slender rods of finite width w. Then the motion of a single rod is again strongly confined by a tube comprised of the surrounding particles. For large aspect ratios L/w the isotropic-nematic spinodal occurs at 3D concentrations $c \approx 4/wL^2$ [22], e.g., at $c = 200/L^3$ for $L/w = 50$. For densities $100 \leq cL^3 \leq 150$, 3D simulations of suspensions of rods with this aspect ratio exhibit significantly anisotropic diffusion of about $25 \leq D_\parallel/D_\perp \leq 50$ [5, 6].

---

[2]To achieve sufficient statistics, we collected at least 350 trajectories for each density. For the largest densities, the simulation of a single trajectory took about 13 days of CPU time on a AMD Opteron® 2.6 GHz core.

T. Munk F. Höfling E. Frey T. Franosch

In our 2D model such ratios are attained for $n^* \approx 20$, already at the onset of the regime of entangled diffusion. Experimental realisations of highly entangled rod suspensions may be achieved, e.g., for the tobacco mosaic virus. Mutants of this rod-shaped virus have been observed with an aspect ratio of 50 and higher [27], thus entangled suspensions below the nematic phase transition should be feasible. Another promising model system are solutions of microtubules; their aspect ratio can even be considerably larger [28, 29], and with a ratio of 100 they can still be considered as approximately stiff rods. A third example are solutions of *fd* viruses, exhibiting a high degree of monodispersity and a comparable aspect ratio of about 130 [16].

In the preceding discussion we have neglected hydrodynamic interactions mediated by the solvent. Inclusion of these effects present a considerable challenge both to the theory and the simulation techniques, and is beyond the scope of our work. The possible influences of hydrodynamic forces are twofold: First, a logarithmic length dependence, $\ln(L/w)$, decorates the microscopic expression for the diffusion coefficients. Since the ratios of $D_\perp$, $D_\parallel$, and $D_{\rm rot}$, are independent of this correction, this effect is already accounted for by choosing $\tau_0 = L^2/D_\parallel^0$ as the basic unit of time, as we have done here. Second, nonadditive hydrodynamic forces between the rods might change the observed dynamics, in particular at short times [30]. Recently, Pryamitsyn and Ganesan [31] have argued on the basis of computer simulations that effects of hydrodynamic interactions on the translational and rotational diffusivity are secondary relative to the steric interactions. Assuming that hydrodynamic interactions merely renormalise the macroscopic transport coefficients, the mechanism of translation-rotation coupling remains unaffected, and our theory should still be applicable.

It is straightforward to extend the concept of an effective Perrin theory to 3D suspensions of long, thin rods since the motion in the tube is essentially one-dimensional. The formal solution is then provided in terms of spheroidal wave functions [8, 20], which serves as a starting point to calculate the intermediate scattering function. In particular, the confined motion of rods is characterised again by a power law decay of the intermediate scattering function, which we predict to $F(\boldsymbol{k}, t) \simeq (4k^2 D_\parallel t/\pi)^{-1/2}$. This algebraic decay constitutes a generic feature of the sliding motion and should be observable directly in scattering experiments.

$$* * *$$

REFERENCES

[1] HAN Y., ALSAYED A. M., NOBILI M., ZHANG J., LUBENSKY T. C. and YODH A. G., *Science*, **314** (2006) 626.
[2] MUKHIJA D. and SOLOMON M. J., *J. Coll. Interf. Science*, **314** (2007) 98.
[3] BHADURI B., NEILD A. and NG T. W., *Appl. Phys. Lett.*, **92** (2008) 084105.
[4] CUSH R., DORMAN D. and RUSSO P., *Macromol.*, **37** (2004) 9577.
[5] COBB P. D. and BUTLER J. E., *J. Chem. Phys.*, **123** (2005) 054908.
[6] BITSANIS I., DAVIS H. T. and TIRRELL M., *Macromol.*, **23** (1990) 1157.
[7] SZAMEL G., *Phys. Rev. Lett.*, **70** (1993) 3744.
[8] OTTO M., ASPELMEIER T. and ZIPPELIUS A., *J. Chem. Phys.*, **124** (2006) 154907.
[9] HÖFLING F., FREY E. and FRANOSCH T., *Phys. Rev. Lett.*, **101** (2008) 120605.
[10] ONSAGER L., *Ann. N. Y Acad. Sci.*, **51** (1949) 627.
[11] ALLEN M. P., *Phys. Rev. Lett.*, **65** (1990) 2881.
[12] LÖWEN H., *Phys. Rev. E*, **59** (1999) 1989.
[13] KIRCHHOFF T., LÖWEN H. and KLEIN R., *Phys. Rev. E*, **53** (1996) 5011.
[14] VAN BRUGGEN M. P. B., LEKKERKERKER H. N. W., MARET G. and DHONT J. K. G., *Phys. Rev. E*, **58** (1998) 7668.
[15] LETTINGA M. P., BARRY E. and DOGIC Z., *Europhys. Lett.*, **71** (2005) 692.
[16] LETTINGA M. P. and GRELET E., *Phys. Rev. Lett.*, **99** (2007) 197802.
[17] PERRIN F., *J. Phys. Radium*, **7** (1936) 1.
[18] BERNE B. J. and PECORA R., *Dynamic Light Scattering* (John Wiley and Sons, New York) 1976.
[19] DOI M. and EDWARDS S. F., *The Theory of Polymer Dynamics* (Oxford University Press, Oxford) 1986.
[20] ARAGÓN S. R. and PECORA R., *J. Chem. Phys.*, **82** (1985) 5346.
[21] HÖFLING F., MUNK T., FREY E. and FRANOSCH T., *Phys. Rev. E*, **77** (2008) 060904(R).
[22] TAO Y.-G., DEN OTTER W. K., DHONT J. K. G. and BRIELS W. J., *J. Chem. Phys.*, **124** (2006) 134906.
[23] HÖFLING F., MUNK T., FREY E. and FRANOSCH T., *J. Chem. Phys.*, **128** (2008) 164517.
[24] ABRAMOWITZ M. and STEGUN I. A., *Handbook of Mathematical Functions* (Harri Deutsch, Frankfurt/Main) 1984.
[25] KÄMMERER S., KOB W. and SCHILLING R., *Phys. Rev. E*, **56** (1997) 5450.
[26] PFLEIDERER P., MILINKOVIC K. and SCHILLING T., *Europhys. Lett.*, **84** (2008) 16003.
[27] MILLER R., PRESLEY A. and FRANCIS M., *J. Am. Chem. Soc.*, **129** (2007) 3104.
[28] GITTES F., MICKEY B., NETTLETON J. and HOWARD J., *J. Cell Biol.*, **120** (1993) 923.
[29] PAMPALONI F., LATTANZI G., JONÁŠ A., SURREY T., FREY E. and FLORIN E.-L., *Proc. Natl. Acad. Sci.*, **103** (2006) 10248.
[30] GUZOWSKI J., CICHOCKI B., WAJNRYB E. and ABADE G. C., *J. Chem. Phys.*, **128** (2008) 094502.
[31] PRYAMITSYN V. and GANESAN V., *J. Chem. Phys.*, **128** (2008) 134901.